Infrared Radiative Properties of Tropical Cirrus Clouds Inferred from Aircraft Measurements

KEITH T. GRIFFITH

Research Aviation Facility, National Center for Atmospheric Research, Boulder, CO 80307

STEPHEN K. COX

Department of Atmospheric Science, Colorado State University, Fort Collins, CO 80523

ROBERT G. KNOLLENBERG

Particle Measuring Systems, Boulder, CO 80301

(Manuscript received 9 April 1979, in final form 5 December 1979)

ABSTRACT

Longwave emissivities and the vertical profile of cooling rates of tropical cirrus clouds are determined using broadband hemispheric irradiance data. Additionally, a broadband mass absorption coefficient is defined and used to relate emissivity to water content. The data used were collected by the National Center for Atmospheric Research (NCAR) Sabreliner during the GARP Atlantic Tropical Experiment (GATE) in the summer of 1974.

Three case studies are analyzed showing that these tropical cirrus clouds approached an emissivity of 1.0 within a vertical distance of 1.0 km. Broadband mass absorption coefficients ranging from 0.076 to 0.096 $m^2 g^{-1}$ are derived. A comparison of these results with other work suggests that tropical cirrus cloud emissivities may be significantly larger than heretofore believed.

Ice water content of the clouds was deduced from data collected by a one-dimensional particle spectrometer. Analyses of the ice water content and the observed particle size distributions are presented.

1. Introduction

Radiative properties of cirrus clouds have been observed by many authors using several different techniques (Brewer and Houghton, 1956; Fritz and Rao, 1967; Kuhn and Weickmann, 1969; Platt, 1973; Platt and Gambling, 1971; Allen, 1971; Davis, 1971). However, information on cloud microphysics has been lacking in each of the above studies. Theoretical studies of the radiative properties of cirrus have been reported by Hunt (1973) and Liou (1974). These theoretical studies must incorporate crucial assumptions about crystal shape and size distribution in cirrus clouds. The present study combines aircraft measurements of cirrus cloud microphysics with simultaneous radiometric observations. This unique data set may serve as a first step toward the coherent merging of observation and theory.

Longwave emissivities and the vertical profile of cooling rates of tropical cirrus clouds are determined using broadband (4–50 μm) hemispheric irradiance data. Additionally, a broadband mass absorption coefficient is defined and used to relate emissivity to water content. These parameters are determined by employing a variation on a broadband infrared radiative transfer routine that was described by Cox (1973). The model requires as input data the vertical structure of upward and downward irradiances, temperature, water vapor, carbon dioxide and cloud-top and cloud-base pressures. The model then performs two basic functions. First, the emissivity of the cloud particles alone is isolated from the effects of water vapor and carbon dioxide in the cloud layer. This differs from the concept of the effective emissivity of the layer (Cox, 1971, 1976; Paltridge, 1974) which does not distinguish between the contributions of the gaseous constituents and the contribution due to the cloud aerosol itself. Second, the model smooths the data into a coherent profile from which cloud emissivities, layer cooling rates and, given the vertical structure of ice water content, broadband mass absorption coefficients are derived.

A complete description of the longwave radiometer, its limitations and the techniques used in reducing the raw data may be found in Albrecht *et al.* (1974) and Albrecht and Cox (1976, 1977). The ice water content information was derived from data

0022-4928/80/051077-11$06.75

TABLE 1. Summary of errors in the calculation of emissivity and mass absorption coefficient resulting from inaccuracies in the measured input parameters.

Parameter	Expected accuracy of data	Resulting emissivity errors	Resulting K errors (%)
Irradiance (Random errors)	± 2 W m^{-2}	± 0.01	± 4
Irradiance (Bias errors)	± 5 W m^{-2}	± 0.05	± 12
Cloud-top and base pressure	± 1.5 mb	± 0.03	± 3
Temperature	± 0.5°C	± 0.02	± 3
Water vapor mixing ratio	$\pm 10\%$	$< \pm 0.01$	$< \pm 1$
Ice water content	$\pm 40\%$	± 0.03	± 40
Maximum cumulative error (90% confidence limits)		± 0.12	± 60

collected by a one-dimensional particle spectrometer. A description of this instrument is given by Knollenberg (1970) and Heymsfield (1976).

2. Broadband infrared radiative transfer model

The purpose of the infrared (IR) numerical transfer model as used in this study is to isolate the radiative effects of the cloud itself from the effects of the water vapor and carbon dioxide and to provide a smoothed, coherent vertical profile of cloud emissivity from the measured irradiances. The IR irradiances calculated by the model are obtained by using the vertical distribution of temperature, water vapor, carbon dioxide and clouds as independent variables in a radiative transfer equation evaluation. Smoothing of the vertical profile of the measured irradiances is accomplished in an iterative manner by adjusting the cloud emissivity in the model calculation until the best match with the observations is obtained. The radiative heating rates are then calculated from the divergence of net radiation based upon the smoothed model irradiance profile.

With the exception of the treatment of cloud and the cloud overlap correction, the basic computational technique for the gaseous constituents follows the method of Cox (1973) and Cox and Griffith (1979a,b). The downward irradiance is given by Eq. (1).

$$H_i\downarrow = \int_0^{p_i} B(T,p)\,\frac{\partial \epsilon_g}{\partial p}\,dp + \int_0^{p_i} B(T,p)\left(\frac{\partial \epsilon_{\mathrm{CLD}}}{\partial p} - \frac{\partial \epsilon_{\mathrm{OVL}}}{\partial p}\right)dp, \quad (1)$$

where

$$\frac{\partial \epsilon_{\mathrm{OVL}}}{\partial p} = \frac{\partial(\epsilon_g \epsilon_{\mathrm{CLD}})}{\partial p}. \quad (2)$$

In the above ϵ_{CLD} is the greybody emissivity of the nongaseous water substance in the column extending from the top of the atmosphere to the level p, ϵ_g is the sum of the integral flux emissivities of the atmospheric gases for the same column minus a gaseous overlap correction, ϵ_{OVL} is the grey cloud-gaseous overlap correction and $B(T,p)$ is the Planck function.

In Eq. (1) the profile of ϵ_{CLD} is the only unknown assuming simultaneous observations of the profiles of the downward irradiance $H_i\downarrow$, temperature and water vapor, and known concentrations of O_3 and CO_2. Furthermore, if one knows the liquid water content (LWC) profile, a greybody mass absorption coefficient may be related to the cloud emissivity through Eq. (3). We assume that the emissivity of the cloud water (non-vapor) may be expressed as an exponential function of z, distance from cloud top or base to the point in question, the LWC (or ice water content IWC) and a greybody mass absorption coefficient K:

$$\epsilon_{\mathrm{CLD}} = 1 - \exp(-K \cdot \mathrm{LWC} \cdot z). \quad (3)$$

Eq. (3) has no rigorous theoretical basis since K should be a function of the particle size distribution and concentration, both of which vary with depth within the cloud. However, Stephens (1978) and Paltridge (1974) have shown that this concept of a constant greybody mass absorption coefficient may be successfully employed to reproduce the essence of the radiative properties of liquid water clouds. On that basis we have adopted Eq. (3) for our analysis. Our results will show that this empirical relation does indeed allow us to computationally reproduce the measured radiative properties of ice clouds.

Eqs. (1) and (3) are then solved iteratively for the value of K which minimizes the difference between the observed irradiance profile $H_i\downarrow_{\mathrm{OBS}}$ and that calculated from the observed data set of independent variables.

SENSITIVITY OF THE MODEL

The model was tested extensively to determine how well the ϵ_{CLD} parameter could be retrieved when the input data contained errors. These errors may be due to instrument errors, inhomogeneities in the meteorological situation or even inaccuracies in observers' notes. It is essential to know how tolerant the model is of these conditions.

The sensitivity testing of the model has shown that the accuracy requirements for the input data are comparable to the expected quality of the real data. Table 1 summarizes the expected magnitude of the errors in cloud emissivity and mass absorption coefficient given errors in the measured variables. Cloud-top and cloud-base data from observers'

notes are normally reliable to within 30 m. Temperature and moisture measurements are quite accurate and climatological data are adequate where measurements are not available. Errors in emissivities and K values resulting from temperature, moisture or cloud-top uncertainties should be 3% or less. Accurate IWC values are critical to the determination of the mass absorption coefficient. The relationship between IWC and K [when Eq. (3) is used to find K from known cloud emissivity and IWC] dictates that any percentage error in IWC will be matched by an equal percentage error of opposite sign in the K value. But emissivities derived from the erroneous IWC values will be accurate to a few percent since the model conserves the $K \cdot$IWC product. The expected precision of the IWC data is estimated as ±40% in Table 1. This uncertainty is due mainly to the necessity of assuming a crystal shape. The measured irradiances will yield K values and emissivities to within a relative error of 4% if only random instrumental error is considered. The effects of concurrent measurement errors in all six relevant variables will result in emissivities within ±0.12 and K values within ±60%.

3. Data collection and reduction

Broadband longwave hemispheric irradiance data were collected by one upward-facing and one downward-facing Eppley Precision Infrared Radiometer (Pyrgeometer). This instrument responds to radiation in the 4–50 μm spectral interval. A description of the NCAR Sabreliner radiation system and details of the radiation data reduction procedures are given by Albrecht and Cox (1976). Detailed reports on the operating characteristics, calibration procedures and theory of operation of pyrgeometers may be found in Albrecht *et al.* (1974) and Albrecht and Cox (1977).

Basically, the values of pressure, temperature, dew point and longwave irradiance for any given level in the atmosphere were obtained from averaging 1 s values on straight and level data collection flight legs. These sampling flight legs varied in length on different dates from 14 min (~170 km) to as little as 75 s (~15 km). However, all data collection flight legs used to construct any given vertical profile are of similar length. Climatological values of pressure, temperature and moisture (Griffith and Cox, 1977) were used at altitudes above and beneath the layers sampled. For in-cloud data flight legs at these very cold temperatures, (−60 to −30°C) the air was assumed to be saturated with respect to ice.

Since the IWC calculation is so central to the derivation of cloud mass absorption coefficients, it will be described in detail. Ice water content values were derived from data collected by a one-dimensional optical array particle spectrometer built by Particle Measuring Systems, Inc. (PMS). This instrument counts and sizes cloud particles into 15 equally spaced size channels in the *nominal range* of 20 to 300 μm. A description of this instrument is given by Knollenberg (1970, 1973). The spectrometer operates on the principle that a cloud particle passing through a laser beam will cast a shadow on a linear array of photodiodes oriented at right angles to the flow. Basically, the number of photodiode elements darkened by the particle is proportional to the particle size.

TABLE 2. The effect of particle shape assumption on calculated IWC for the measured size distribution of Fig. 1.

Shape assumption		Calculated IWC (g m^{-3})
Spheres	(100%)	0.0703
Columns	(100%)	0.0818
Rosettes	(100%)	0.0348
Small Snow	(100%)	0.0350
Columns and Rosettes	(50%) (50%)	0.0583

The design of the probe dictates that spherical particles are sized and counted more accurately than any other shape. Since the particles in cirrus clouds are usually columns and/or bullet rosettes (Heymsfield and Knollenberg, 1972), a systematic error is introduced into the probe measurements, and consequently the cirrus crystals are undersized and undercounted. Heymsfield (1976) gives a very readable explanation of why the instrument responds in this manner. Knollenberg (1975) evaluated this systematic error in the particle spectrometer. His report details the theoretical probe response to particles of different shapes along with laboratory and field studies aimed at quantitatively defining the relationship between indicated and actual particle size. He shows that the probe is highly sensitive to particle shape. For instance, the corrected size of a spherical particle counted in the 200 μm nominal channel would be 202.7 μm. If that same count represented a column of 4:1 aspect ratio, the corrected size would be 250.0 μm. Hence it is quite important to have some information on what type of particles were sampled by the probe.

No data concerning crystal habit were collected by the Sabreliner on the GATE missions. In the reduction of the PMS probe data, we assume that the particles were 50% columns and 50% bullet rosettes. This yields IWC values about midway between the maximum and the minimum that are possible with various crystal habit assumptions. Table 2 shows the effect of crystal shape assumption on the IWC calculation. This table uses the measured size distribution shown later in Fig. 1.

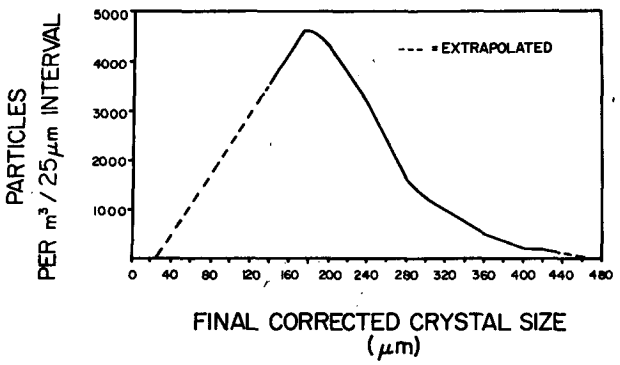

FIG. 1. Particle size distribution for Day 226, 10 400 m. Combined rosettes (50%) and columns (50%).

The PMS probe is designed and calibrated for use at aircraft speeds of 100 m s^{-1}. At faster speeds the particles transit the photodiode array too quickly for proper instrument response, and undersizing results. An empirical correlation for this shortcoming was made using

$$CSF = CS1 + 50\ \mu m(TAS - 100)/100, \quad (4)$$

where TAS is the aircraft true air speed (m s^{-1}), CS1 is the corrected size (Knollenberg, 1975) and CSF is the final corrected particle size. Since the Sabreliner generally operated at speeds of 180–210 m s^{-1}, the entire spectrum is shifted to larger diameters by an average of 40–55 μm. This implies that the instrument was actually measuring particles as large as 460 μm instead of the theoretical maximum of 300 μm. On the other hand, all particles $\lesssim$ 70 μm were not counted by the instrument.

Based on the above reasoning we can deduce the true size (length) of the crystal. However, because of the somewhat irregular shape of the crystals, variable densities and variable aspect ratios, a conversion from crystal size to equivalent water drop diameter is needed. Results from Knollenberg (1975) were used to construct a table relating a count in a given nominal size channel to the equivalent water drop diameter.

Measured IWC was adjusted upward to account for the fact that there were particles both above and below the size range of the instrument. The plots of IWC versus final corrected particle size were extrapolated to both larger and smaller sizes for selected legs on each day and the average correction added to all the legs on that day. A sample of a typical particle size distribution and the resulting IWC distribution is given in Figs. 1 and 2. Fig. 1 is a graph of particle concentrations as a function of final corrected particle size for the data flight leg at 10.4 km on Julian Day 226 of the 1974 GATE experiment. Fig. 2 is a graph of IWC versus final corrected particle size derived from Fig. 1. The dashed lines in each figure show the extrapolation used outside of the measured portion of the spectrum. Note that in both figures the peak of the distribution and the bulk of the curve are well contained within the measured boundaries. Consequently, we have assumed that we have accounted for most of the IWC and that only a small correction term will be necessary.

It is possible that the number of particles in the small size channels is very much greater than detected here. Fig. 1 depicts the assumption we have made that the particle density drops linearly to zero from the measured peak near 180 μm. If, in fact, the curve rises exponentially for crystal sizes < 140 μm, there may be significant amounts of IWC contributed by these smaller sizes. Such an exponential particle distribution was in fact reported by Heymsfield (1975). We have chosen in this study to use the extrapolation illustrated in Fig. 1. Further discussion of the effects of having significant amounts of IWC outside of the measured size range is given in Section 5.

The pressure level at which the spectrometer first transitioned from clear to cloud or vice versa was used as cloud top or base as appropriate. This was checked against observers' notes to insure consistency.

Typical size distributions for three separate flight legs, assuming that the particles are hexagonal columns of 4:1 ratio, are shown in Fig. 3. Fig. 3 displays only the number of actual measured particles as a function of final corrected crystal size. No extrapolated data are included. Displayed in the figure are two flight legs on Day 232, one at 12.2 km and one at 11.0 km, and one flight leg on Day 251 at 12.8 km. The variation from one level to another is shown by the two flight legs on Day 232 and the similarity from day to day is shown by comparing the distributions for Days 251 and 232. In both figures the curves have been normalized to the same total number of particles so that the spectra may be more directly compared. There is apparently very little difference in the size spectra from day to day

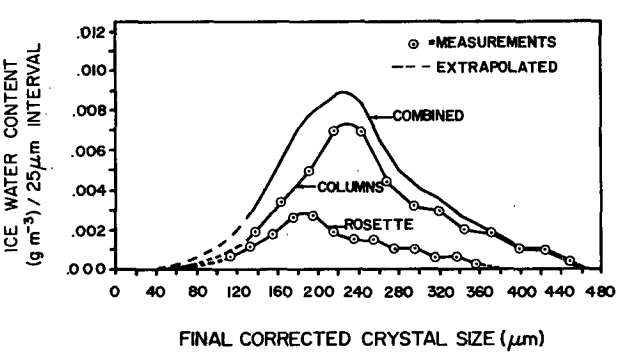

FIG. 2. Ice water content as a function of particle size for a mixture of columns (50%) and rosettes (50%) for Day 226, 10 400 m.

or from one level to another on the same day. The main differences in IWC, and therefore longwave radiative properties, are due to the different concentrations of particles.

4. Case studies

Three separate cases of cirrus cloud decks were investigated. Each case is identified by the Julian Day on which the mission was flown during the GATE experiment. In all instances, the patterns flown were straight and level flight legs through the sampling area followed by descending 180° turns to the next altitude. The length of the data legs on different days ranged from a minimum of ~80 s (16 km), Day 226, to a maximum of 14 min (170 km), Day 251. Sampled altitudes varied for the three days but ranged from a high of 13.1 km to a low of 6.1 km. An irradiance measurement was obtained above cloud top on all three occasions but data below cloud base were not gathered. The cloud systems themselves varied in type from a very tenuous, patchy layer (Day 232) to a dense cirrus anvil outflow from an active cumulonimbus cell (Day 251).

Detailed inspection of the IWC on each data flight leg on Days 232 and 251 revealed that the aircraft was totally out of cloud for a portion of every run. Hence, these cases did not fit the desired ideal of a horizontally homogeneous situation and a different method of analysis was needed. The irradiance data at each level were stratified into three categories: the top 10% of the range, the bottom 10% of the range and all the remaining values. The top 10% of the range category was used to calculate the cloud emissivities and mass absorption coefficients.

The rationale for using this procedure is that a broken cloud condition should produce a nearly binary instrument response. For instance, the highest downward irradiance values should occur while in the cloud and the lowest values should occur while in clear air. There will be a region of intermediate values where the hemispheric field of view of the instrument will sense both clear and cloudy regions. Using the criteria of 10% of the range requires that only one-tenth of the flight leg be typical of the cloudy area or of the clear area. The implicit assumption is also made that the cloudy areas are correlated in the vertical. That is, the maximum downward irradiance at one level must be related to the same cloud situation that produced the maximum downward irradiance at another level. One test of this hypothesis is whether or not the maximum IWC on each leg occurs at the same time as the maximum downward irradiance. In these cases, all but one of the in-cloud data flight legs satisfied this test. The one flight leg that did not had only slightly smaller IWC than the maximum at the time of highest downward irradiance.

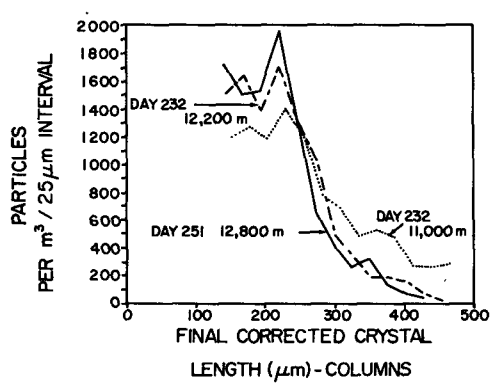

FIG. 3. Measured particle size distribution for three data flight legs with total number of particles normalized to 10 000 m^{-3} and for assumed column shape.

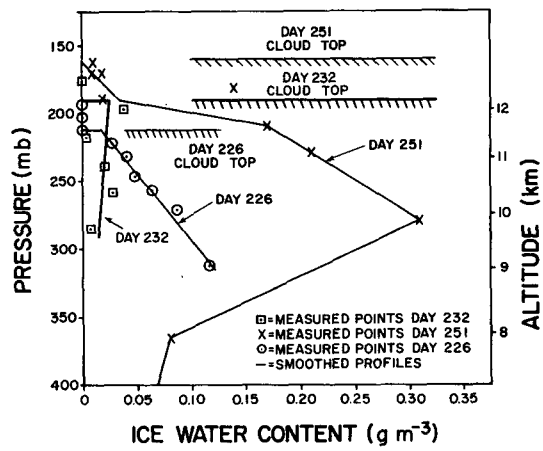

FIG. 4. Vertical structure of ice water content for the three case studies.

The smoothed profiles of IWC along with actual measured points for each of the three cases are depicted in Fig. 4. These profiles were derived under the assumptions described in Section 3 and, for Days 232 and 251, using the stratification technique described here. The Day 226 case exhibited the most organized structure, with IWC increasing uniformly with depth below cloud top. By contrast, the Day 232 case shows no coherent pattern at all, and has the lowest values of IWC of the three cases. This is indicative of the thin, patchy, disorganized nature of this cloud system. The Day 251 profile was drawn to indicate a slightly higher IWC at the 12.2 km level than was actually measured. This was necessary because examination of the flight film indicated that there was a somewhat layered structure to the cloud. The integrated smoothed profile is intended to provide a more accurate representation of the total column water content than would be obtained from strict interpretation of the 12.2 km IWC measurement. There is a rather sharp transition between the flight leg at 12.2 km and the flight leg

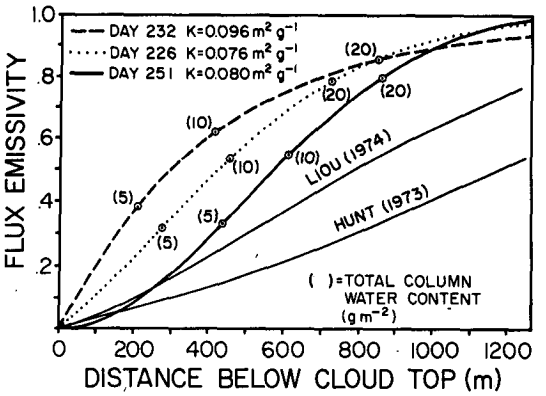

FIG. 5. Vertical profile of emissivity within the cloud layer for each of the three case studies with comparisons to Hunt (1973) and Liou (1974).

at 11.6 km. The four data points at 12.2 km and above are similar in magnitude to the values found on Days 226 and 232. The points below that are over three times as large as any of our previous cirrus IWC measurements (0.3 g m^{-3}). This clearly suggests that the lower portions of this cloud system contained an active cell.

Emissivity as a function of distance below cloud top is displayed in Fig. 5 for each of the three cases. Also indicated are the mass absorption coefficients derived from the downward irradiance data and the total column water content at values of 5, 10 and 20 g m^{-2}. The results for all three days are quite similar with the cirrus clouds approaching an emissivity of 1 in a depth of 1–1.2 km. The shapes of the curves in approaching the limiting value reflect the differences in the IWC profiles on different days. This can be seen by noting that the total column water content values (in parentheses) for the three cases lie very nearly in horizontal lines corresponding to single emissivity values.

For comparison, a curve obtained from the theoretical calculations of Hunt (1973) is shown. Although Hunt's calculations were performed for a wavelength of 10 μm, it is instructive to compare the two sets of results. This curve uses Hunt's Table 2(i) for ice spheres of 50 μm modal radius with the optical depth versus distance below cloud-top relation derived from the IWC profile of the Day 226 case. The Hunt curve shows a lower emissivity than the measured cases at all depths into the cloud. There are several possible explanations for this disagreement. The most likely relates to the difference in extinction coefficient for spherical particles as opposed to the irregularly shaped columns, bullet rosettes or other crystalline forms found in real cirrus. Hunt assumes spherical ice particles in compiling his tables. However, it is pointed out by Liou (1974) that the extinction cross section of cylinders is about 1.5 times greater than for spheres of the same volume. Of course, optical depth is directly proportional to this extinction coefficient. If the extinction efficiency of the real cirrus were approximately 5 times the value for spheres the Hunt curve would be reasonably close to agreement with the measured curve. This large an extinction efficiency factor is not inconceivable considering the probable mix of cirrus crystal forms and their large range of sizes compared to the sizes assumed by Hunt.

A second comparison curve is shown which is derived from the work of Liou (1974). This curve was obtained by deriving a mass absorption coefficient from Liou's Fig. 6, converting it for use with a flux emissivity relation, and applying the IWC profile of Day 226. Hence, as with the Hunt comparison curve, total column water content as a function of distance below cloud top is similar to the measured cases. The Liou curve lies between the present measurements and the Hunt curve, presumably due to the larger extinction coefficients used by Liou.

Fig. 6 depicts emissivity as a function of the total water content of the column above the point of measurement for each of the three cases. This column water content (g m^{-2}) is simply a vertical integration of the ice water content (g m^{-3}). This figure depends, of course, on the crystal habit assumption made in deriving ice water content as described in Section 3. Section 5 examines the effects of making some alternate assumptions about the IWC. Since the mass absorption coefficients are inversely proportional to the total column water content, there is uncertainty in the K value due to the placement of the IWC curves. The plots in Fig. 4 were determined, in some cases somewhat subjectively, to be the most reasonable representation of the IWC in the maximum downward irradiance areas. However, even the most extreme assumptions of IWC profiles would have yielded mass absorption coefficients in the

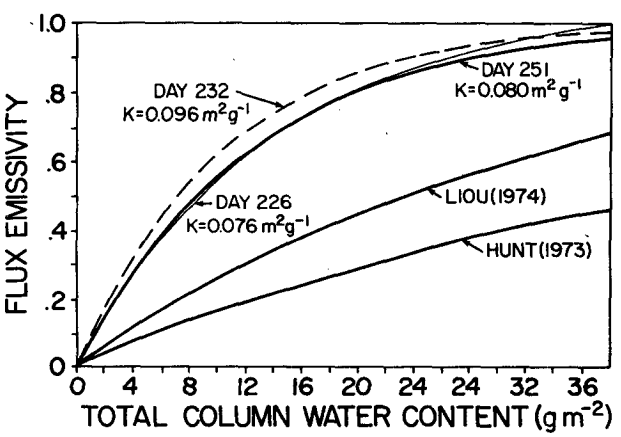

FIG. 6. Relationship between flux emissivity and total column water content for each of the three case studies with comparisons to Hunt (1973) and Liou (1974).

range of 0.060 m^2 g^{-1} (for maximum IWC) to 0.120 m^2 g^{-1} (for minimum IWC).

Comparison curves obtained from Hunt (1973) and Liou (1974) are displayed. Again, both theoretical curves are substantially lower than the measured values. This suggests that the naturally occurring cirrus crystals have greater extinction efficiencies than the spherical ice crystals of Hunt or the uniform cylinders of Liou.

The possibility was considered that significant IR reflectivity of the cloud could be augmenting the downward irradiance and producing this discrepancy between theory and observations. If one assumes that the cloud reflectivity is the same for both the upward and downward irradiance, the net gain in the downward irradiance is equal to the difference between the upward and downward irradiances multiplied by the reflectivity factor. When there is little difference between the two, as in these cases, there can be little net gain in the downward for typical cloud reflectivity of 5% or less. Clearly, this effect can be important in some situations such as at the base of dense cirrostratus with a warm underlying surface. Feigel'son (1970) and Platt (personal communication) have noted that longwave reflectivity can cause the downward IR radiation from such a cloud to exceed blackbody radiation at the cloud temperature.

Heating rates as a function of pressure for the three cases are displayed in Fig. 7. To aid in making the comparison, the curves have been normalized to a common cloud-top location. The smoothed curves were computed from the irradiances generated using the K values retrieved by the model. The K value was derived from the downward irradiances only, but that same K value was used to generate the smoothed upward fluxes. This demonstrates that the derived mass absorption coefficient produces reasonable results for the upward irradiance. The top layer in the cloud shows a cooling maximum of approximately the theoretically predicted magnitude followed by decreased cooling deeper into the cloud.

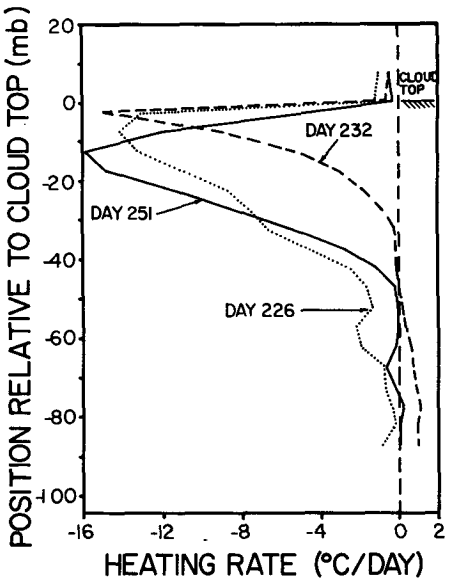

FIG. 7. Vertical distribution of heating rate relative to cloud top.

SUMMARY OF CASE STUDIES

There are substantial similarities in the properties of the tropical cirrus clouds studied on the three different days. Broadband hemispheric mass absorption coefficients fell in the rather narrow range of 0.076 to 0.096 m^2 g^{-1}. Heating rates as a function of pressure were quite uniform both in general shape and in the magnitude of the cloud-top cooling maximum. The measured particle size distributions did not vary substantially from day to day or at different levels on the same day. Hence, the differences in cooling rate profile and emissivity versus distance cannot be attributed to size distribution but rather must be a result of number density variations and its consequent effect on cloud water content.

5. Possible explanations of the discrepancy between theory and observation

Several of the figures describing the results of the individual case studies have pointed out the large differences between the present results and the calculations of Liou (1974) and Hunt (1973). These differences are much larger than one would expect to arise from the different spectral bandpasses represented by our data and those utilized by Hunt. Also, since we have scaled Liou's and Hunt's results to account for the different ice water content, we would expect better agreement between our results and theirs than the preceding analysis shows. There are at least three plausible explanations: the cloud contains significant quantities of small liquid water droplets; inadequacies in the determination of ice water content; and preferential orientation and types of ice crystals assumed in the theoretical studies.

Comparisons to theoretical studies of ice clouds have been made in previous figures. Fig. 8 compares the current results of emissivity vs total water content for ice clouds to three theoretical studies of typical liquid water clouds (Hunt, 1973; Zdunkowski and Crandall, 1971; Yamamoto *et al.*, 1970). The figure illustrates that there is disagreement among various authors about the proper emissivity relationship even for similar liquid water content and drop size distribution. It is recognized, however, that the study of Zdunkowski and Crandall and the study of Hunt are spectral (10.6 and 11.0 μm, respectively) and that the work of Yamamoto *et al.*,

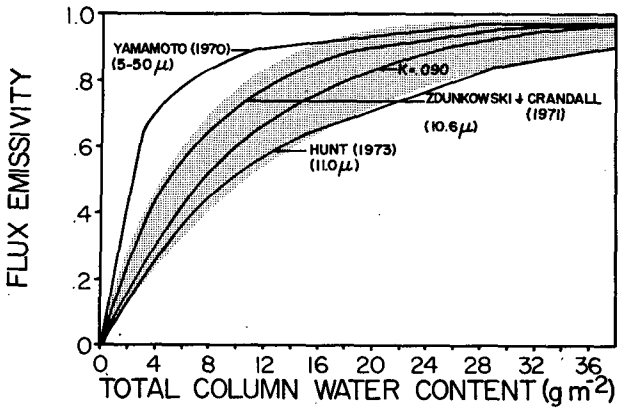

FIG. 8. Comparison between the present study and theoretical estimates of flux emissivity for *water* clouds of similar LWC and drop size distribution. (Stippled area indicates uncertainty in present observations.)

is broadband, covering 5 to 50 μm. This may account for most of the differences between the curves. It is curious that the radiative characteristics of the dense tropical cirrus clouds reported in this study are more similar to water clouds than to the results of Hunt and Liou for ice clouds. However, since the air temperature was -55°C or colder for all of the observations reported in this study, we must abandon the tempting explanation that our observations might have been made in the presence of supercooled water droplets.

Section 3 described the procedures used and the assumptions made in deriving the IWC profiles in Fig. 4. If, however, we make different assumptions regarding the extrapolated portion of the particle spectra, significantly different total IWC values can

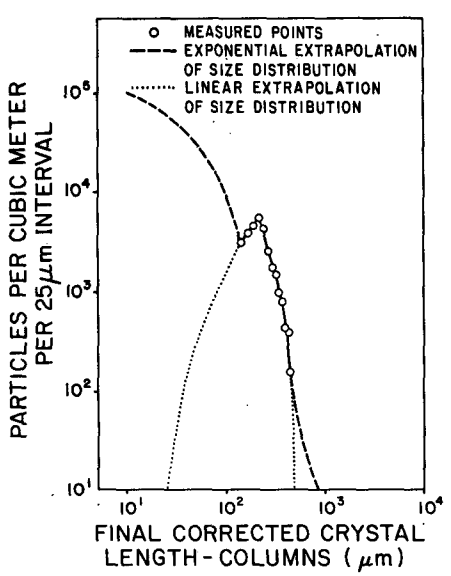

FIG. 9. Particle size distribution for Day 226, at an altitude of 10 400 m.

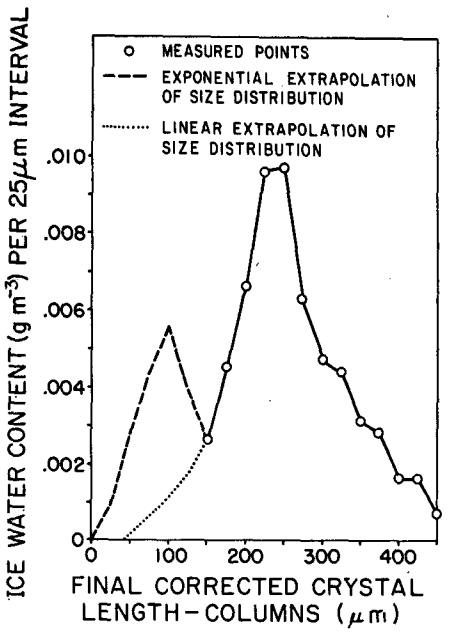

FIG. 10. Ice water content as a function of particle size for Day 226, at an altitude of 10 400 m.

be obtained. Heymsfield (1975, 1976) and Heymsfield and Knollenberg (1972) show particle spectra that indicate an exponential relation in the number of very small particles present. Fig. 9 shows such an exponential extrapolation of particles per cubic meter for the same measured distribution illustrated in Fig. 1. Fig. 10 shows IWC versus particle size for the size distribution of Fig. 9. A distinct secondary maximum results and causes an increase of ~40% in the total IWC when compared to the identical data set with the extrapolation illustrated in Fig. 2. Similar percentage increases in total IWC were found for other data flight legs on the three days studied.

The effect of this change in IWC on the retrieval of mass absorption coefficients and emissivities is discussed in general terms in Section 2. Specifically, the K values derived based on the IWC profiles given in Fig. 5 would be too high. The relationship of inverse proportionality between IWC and K would dictate that for a uniform 40% increase in IWC, the previous K value would have to be divided by 1.40. This adjustment would bring better agreement between observation and theory.

The possible existence of numerous small particles may significantly alter the extinction efficiency of the entire distribution. Paltridge and Platt (1976) discuss the effect of the Mie size parameter ($2\pi R/\lambda$) on the extinction efficiency of spheres. A weighted average performed for the two extrapolated size distributions reveals that the extinction efficiency, at least for equivalent spheres, changes very little, remaining close to 2.

A second reasonable explanation for the differences between observation and theory concerns the question of crystal type and orientation. It is an accepted fact that cirrus particles are not spherical. The differences between the theoretical work of Hunt (1973) who assumed ice spheres, and Liou (1974) who used randomly oriented ice cylinders, are due largely to this shape difference. The discussion here will deal with the effect of Liou's assumption of random orientation of the ice cylinders.

Fluid dynamical considerations dictate that cylindrical crystals present the most resistance to motion while falling. This in turn dictates that the crystals fall with their long axis oriented horizontally. Platt (personal communication) reported observations of lidar backscatter from high cirrus layers which indicated a coherent crystal orientation pattern in some instances. The occurrence of distinct optical phenomena such as sundogs confirm that there is some uniformity of crystal orientation, at least occasionally. This means that the cross-sectional area in a horizontal plane of a large number of cylindrical crystals would be much greater for the preferential orientation case than for the random orientation assumed by Liou. If one assumes that the emissivity change would be proportional to the cross-sectional area, then the magnitude of this effect is on the order of a factor 1.5–2.0. This would allow the Liou curve to move upward to within the envelope of uncertainty of the values derived from observations.

6. Comparison to other observational studies

Measurements of the intensity emissivity of cirrus clouds have been reported by several authors. The flux emissivity measurements reported in this study have been adjusted to intensity emissivity by using a diffusivity factor of 1.6 (Paltridge and Platt, 1976); a comparison between the present measurements and other reported values is shown in Fig. 11. Note that this figure displays emissivity as a function of depth into the cloud. None of the other studies had direct measurement of IWC available to them, thus a more direct comparison of emissivity vs total water content is not possible. The studies of Platt (1973), Davis (1971) and Brewer and Houghton (1956) show emissivity values in the same general range as observed in this study. There is a broad range of observed values, however. The extensive study of Kuhn and Weickmann (1969) indicates much lower emissivities. None of their values approach 1.0 even for 5 km thick cirrus. In addition, most of the emissivity values observed by Platt (1973) would agree reasonably well with Kuhn and Weickmann. Platt, however, did not observe the strong correlation between cirrus thickness and emissivity found by Kuhn and Weickmann. Thus, Platt found emissivities

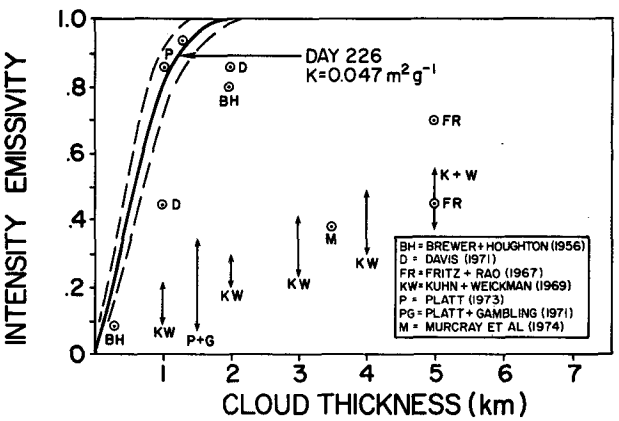

FIG. 11. Comparison of the results of the present study with the observations reported by other investigators. (Dashed line envelope indicates uncertainty of Day 226 observations from present study.)

ranging from less than 0.1 to approximately 0.9 for 1 km thick cirrus. This is probably due to the natural variability of cirrus cloud particle density. If the various measurements of emissivity could be referenced to some bulk cloud property such as water content, certainly much of the scatter in the observations would disappear.

There are two other studies (Allen, 1971; Valovcin, 1968) which also reported cirrus emissivities that on occasion would approach unity. They have not been included in Fig. 11 because cloud thickness information was not available. It should be noted that the mean emissivities reported by Valovcin and by Allen were much less than unity. For instance, Allen reported a mean cirrus emissivity of ~0.35. This is further indication of the wide variability of cirrus emissivity.

It is not surprising, then, that the cirrus clouds sampled in this study were found to lie on the high end of observed emissivities. These clouds were produced from recent and/or continuing convective activity in a moist tropical environment. It is quite possible that the clouds sampled were not even in an equilibrium state due to their close proximity in space and time to the generation cell. One might then expect them to be more dense than the mid-latitude cirrus reported by Kuhn and Weickmann.

7. Conclusions

Longwave emissivities and the vertical profile of cooling rates of tropical cirrus clouds are determined using broadband (4–50 μm) hemispheric irradiance data. Additionally, a broadband mass absorption coefficient is defined and used to relate emissivity to water content. These parameters are determined by employing a variation on a broadband IR radiative transfer routine that was described by Cox (1973). This model has been used to analyze

data collected by the National Center for Atmospheric Research (NCAR) Sabreliner during the GARP Atlantic Tropical Experiment (GATE) in the summer of 1974.

Three cases of high tropical cirrus clouds were analyzed. It was found that these clouds approached an emissivity of 1.0 in a vertical distance of 1–1.2 km. Comparison of these results with the theoretical results of Hunt (1973) and Liou (1974) revealed large differences. Both of these theoretical studies predict emissivities of less than 1.0 even at over 6 km into the cloud.

Mass absorption coefficients ranging from 0.076 $m^2\ g^{-1}$ for Day 226 to 0.096 $m^2\ g^{-1}$ for Day 232, with an average of 0.084 $m^2\ g^{-1}$ were derived. Again, comparison of emissivities versus total column water content between the theoretical results of Hunt (1973) and Liou (1974) and the present study reveal large differences. It is suggested that the large irregular particles of real cirrus clouds have significantly greater extinction efficiencies than the spheres of Hunt's study or the regular columns of Liou's study.

Further comparison is made with measurements of cirrus emissivities reported by other authors. A wide range of observational results have been reported. The studies of Platt (1973), Davis (1971) and Brewer and Houghton (1956) have some measurements in the same general range as the present study. However, the study of Kuhn and Weickmann (1969) reported no cirrus emissivities as high as those found in this research. These differences are probably due to the natural variability of cirrus cloud properties. If all of these diverse measurements could be referenced to the water content of the clouds, most of the differences would probably be resolved.

Theoretical curves of emissivity as a function of column water content for liquid water clouds compiled by Yamamoto *et al.* (1970), Zdunkowski and Crandall (1971) and Hunt (1973) are compared to the results for ice clouds reported here. This comparison indicates that perhaps the differences in radiative properties of water clouds and ice clouds veiling the tropical cloud cluster are not as great as indicated by theoretical studies.

The IR radiative heating rates within the cloud layer for these cirrus clouds are similar to those of lower cloud layers. The typical cloud-top cooling maximum followed by essentially neutral heating rates deeper into the cloud were observed. The magnitude of the cooling maximum at cloud top ranged from 12 to 16°C day^{-1} and the exact location of the cooling peak was shown to be modulated by the IWC structure near cloud top.

Acknowledgments. This research has been supported in part by the following agencies: the Global Atmosphere Research Program, National Science Foundation, and the GATE Project Office, NOAA, under Grant ATM 78-05743, and the National Aeronautics and Space Administration under Grant NSA 5357.

We wish to acknowledge the Research Aviation Facility and the Computing Facility of the National Center for Atmospheric Research which is sponsored by the National Science Foundation.

REFERENCES

Albrecht, B., and S. K. Cox, 1976: Radiation data reduction procedures for Sabreliner, C-130, and DC-6 aircraft during the GARP Atlantic Tropical Experiment. Atmos. Sci. Pap. No. 244, Colorado State University [NTIS PB257375/AS].

——, and S. K. Cox, 1977: Methods for improving pyrgeometer measurements. *J. Appl. Meteor.*, **16,** 188–197.

——, M. Poellot and S. K. Cox, 1974: Pyrgeometer measurements from aircraft. *Rev. Sci. Instrum.*, **45,** 33–38.

Allen, J. R., 1971: Measurements of cloud emissivity in the 8–13 μ waveband. *J. Appl. Meteor.*, **10,** 260–265.

Brewer, A. W., and J. T. Houghton, 1956: Some measurements of the flux of infra-red radiation in the atmosphere. *Proc. Roy. Soc. London*, **A236,** 175–186.

Cox, S. K., 1971: Cirrus clouds and the climate. *J. Atmos. Sci.*, **28,** 1513–1515.

——, 1973: Infrared heating calculations with a water vapor pressure broadened continuum. *Quart. J. Roy. Meteor. Soc.*, **99,** 669–679.

——, 1976: Observations of cloud infrared effective emissivity. *J. Atmos. Sci.*, **33,** 287–289.

——, and K. T. Griffith, 1979a: Estimates of radiative divergence during Phase III of the GARP Atlantic Tropical Experiment: Part I. Methodology. *J. Atmos. Sci.*, **36,** 576–585.

——, and ——, 1979b: Estimates of radiative divergence during Phase III of the GARP Atlantic Tropical Experiment: Part II. Analysis of Phase III results. *J. Atmos. Sci.*, **36,** 586–601.

Davis, P. A., 1971: Applications of an airborne ruby lidar during a BOMEX Program of cirrus observations. *J. Appl. Meteor.*, **10,** 1314–1323.

Feigel'son, E. M., 1970: *Radiant Heat Transfer in a Cloudy Atmosphere.* Israel Program for Scientific Translations, 191 pp.

Fritz, S., and P. Krishna Rao, 1967: On the infrared transmission through cirrus clouds and the estimation of relative humidity from satellites. *J. Appl. Meteor.*, **6,** 1088–1096.

Griffith, K. T., and S. K. Cox, 1977: Infrared radiative properties of tropical cirrus clouds inferred from broadband measurements. Atmos. Sci. Pap. No. 269, Colorado State University [NTIS PB 26853].

Heymsfield, A. J., 1975: Cirrus uncinus generating cells and the evolution of cirriform clouds. Part I: Aircraft observations of the growth of the ice phase. *J. Atmos. Sci.*, **32,** 799–808.

——, 1976: Particle size distribution measurement: An evaluation of the Knollenberg Optical Array Probes. *Atmos. Tech.*, No. 8. 17–24, NCAR.

——, and R. G. Knollenberg, 1972: Properties of cirrus generating cells. *J. Atmos. Sci.*, **9,** 1358–1366.

Hunt, G. E., 1973: Radiative properties of terrestrial clouds at visible and infrared thermal window wavelengths. *Quart. J. Roy. Meteor. Soc.*, **99,** 346–369.

Knollenberg, R. G., 1970: The optical array: An alternative to scattering or extinction for airborne particle size determination. *J. Appl. Meteor.*, **9,** 86–103.

——, 1973: Measurements of the growth of the ice budget in a persisting contrail. *J. Atmos. Sci.*, **29,** 1367–1374.

——, 1975: The response of optical array spectrometers to ice

and snow: A study of probe size to crystal mass relationships. Air Force Cambridge Research Laboratories, AFCRL-TR-75-0494.

Kuhn, P. M., and H. K. Weickmann, 1969: High altitude radiometric measurements of cirrus. *J. Appl. Meteor.*, **8,** 147–154.

Liou, K., 1974: On the radiative properties of cirrus in the window region and their influence on remote sensing of the atmosphere. *J. Atmos. Sci.*, **31,** 522–532.

Murcray, D. G., J. N. Brooks, F. H. Murcray and W. J. Williams, 1974: 10 to 12 μm spectral emissivity of a cirrus cloud. *J. Atmos. Sci.*, **31,** 1940–1942.

Paltridge, G. W., 1974: Infrared emissivity, short-wave albedo, and the microphysics of stratiform water clouds. *J. Geophys. Res.*, **79,** 4053–4058.

——, and C. M. R. Platt, 1976: *Radiative Processes in Meteorology and Climatology*. Elsevier, 318 pp.

Platt, C. M. R., 1973: Lidar and radiometric observations of cirrus clouds. *J. Atmos. Sci.*, **30,** 1191–1204.

——, and D. J. Gambling, 1971: Emissivity of high layer clouds by combined lidar and radiometric techniques. *Quart. J. Roy. Meteor. Soc.*, **97,** 322–325.

Stephens, G. L., 1978: Radiation profiles in extended water clouds. II. Parameterization schemes. *J. Atmos. Sci.*, **35,** 2123–2132.

Valovcin, F. R., 1968: Infrared measurements of jet-stream cirrus. *J. Appl. Meteor.*, **7,** 817–826.

Yamamoto, G., M. Tanaka and S. Asano, 1970: Radiative transfer in water clouds in the infrared region. *J. Atmos. Sci.*, **27,** 282–292.

Zdunkowski, W. G., and W. K. Crandall, 1971: Radiative transfer of infrared radiation in model clouds. *Tellus*, **23,** 517–527.